BIOPHYSICS

Molecular recognition of human islet amyloid polypeptide assembly by selective oligomerization of thioflavin T

Lanlan Yu[1,2], Wenbo Zhang[1], Wendi Luo[3,4], Robert L. Dupont[5], Yang Xu[5], Yibing Wang[6], Bin Tu[3], Haiyan Xu[2], Xiaoguang Wang[5], Qiaojun Fang[3]*, Yanlian Yang[3], Chen Wang[3], Chenxuan Wang[1]*

Selective oligomerization is a common phenomenon existing widely in the formation of intricate biological structures in nature. The precise design of drug molecules with an oligomerization state that specifically recognizes its receptor, however, remains substantially challenging. Here, we used scanning tunneling microscopy (STM) to identify the oligomerization states of an amyloid probe thioflavin T (ThT) on hIAPP$_{8–37}$ assembly to be exclusively even numbers. We demonstrate that both adhesive interactions between ThT and the protein substrate and cohesive interactions among ThT molecules govern the oligomerization state of the bounded ThT. Specifically, the work of the cohesive interaction between two head/tail ThTs is determined to be 6.4 k_BT, around 50% larger than that of the cohesive interaction between two side-by-side ThTs (4.2 k_BT). Overall, our STM imaging and theoretical understanding at the single-molecule level provide valuable insights into the design of drug compounds using the selective oligomerization of molecular probes to recognize protein self-assembly.

INTRODUCTION

Oligomerization is one of the fundamental principles by which nature creates versatile biologically relevant systems (*1*–*3*). At the submolecular level, two, three, or four α-helical strands can pack parallel or antiparallel to form a bundle called a coiled-coil, which is widespread in protein structures (*1*, *4*). At the intermolecular level, multiple proteins can cluster into homo- and hetero-oligomeric complexes to exert their functionalities (*2*, *5*, *6*). In particular, most of the soluble and membrane-bound proteins in a living cell are found to be oligomeric complexes with two or more protein subunits, e.g., the protein kinases, scaffolding proteins, transmembrane receptors, and signaling proteins (*3*, *6*, *7*). The evolutionary selection of oligomeric clusters improves the stability of proteins against proteolytic degradation, increases local protein concentration, enables allosteric cooperativity, and renders high specificity during molecular recognition (*3*). Motivated by the prevalence of protein oligomerization in nature, a key question that emerges is whether such selective oligomerization can be leveraged in the design of drug or labeling molecules, i.e., drug ligands that act as a mimic of native proteins that selectively oligomerize into a cluster to interact with their receptors.

Clustering of ligands and targeted receptors is an important proof of concept in the field of drug design because it conveys the information that drug oligomers can function as an indivisible unit, which differs from the conventional lock and key model where a single drug molecule incorporates into the grooves or channels formed by the successive side chains protruding from the protein surface (*8*, *9*). An understanding of the factor that controls the self-association of drug ligands upon binding, however, is unclear, and thus, a rational engineering of oligomerization state specificity in the target recognition process remains elusive (*3*, *7*). Typically, the oligomerization state of the bound drugs reflects the interplay between a pair of intermolecular interactions—the adhesive interactions between the drug ligand and the protein substrate to dissociate the drug oligomers, and the cohesive interactions among drug molecules to facilitate clustering (*10*). Given the fact that the microenvironment of the binding site fundamentally determines the adhesive interactions, we hypothesize that it is reasonable to engineer the association state of bounded drugs by changing the physiochemical features of the microenvironment.

Here, we first provide experimental evidence that thioflavin T (ThT), a molecular probe used to detect the presence of β-rich amyloid aggregate that is regarded as a diagnostic of protein-misfolding diseases (*11*–*14*), displays an oligomerization state specificity when incorporated into its amyloidal protein receptor, the 8–37 segment of human islet amyloid polypeptide (hIAPP$_{8–37}$; Fig. 1A). In our experiments, hIAPP$_{8–37}$ self-assembled into a two-dimensional β sheet polypeptide monolayer on a freshly cleaved highly oriented pyrolytic graphite (HOPG) surface for ThT adsorption. We used scanning tunneling microscopy (STM) to investigate the adsorption structure of ThT molecules atop hIAPP$_{8–37}$ at a single-molecule level and to map the local electron density of states in real space. To the best of our knowledge, these results are the first experimental evidence to establish the correlation between the intermolecular interactions and the oligomerization state of bound ThT and hint at the principles by which heterogeneous protein-drug complexity can be detected.

[1]State Key Laboratory of Medical Molecular Biology, Institute of Basic Medical Sciences, Chinese Academy of Medical Sciences and Peking Union Medical College, Beijing 100005, P. R. China. [2]Institute of Basic Medical Sciences, Chinese Academy of Medical Sciences, School of Basic Medicine, Peking Union Medical College, Beijing 100005, P. R. China. [3]CAS Key Laboratory of Biological Effects of Nanomaterials and Nanosafety, CAS Key Laboratory of Standardization and Measurement for Nanotechnology, Laboratory of Theoretical and Computational Nanoscience, CAS Center for Excellence in Nanoscience, National Center for Nanoscience and Technology, Beijing 100190, P. R. China. [4]Sino-Danish Center for Education and Research, University of Chinese Academy of Sciences, Beijing 100190, P. R. China. [5]William G. Lowrie Department of Chemical and Biomolecular Engineering, The Ohio State University, Columbus, OH 43210, USA. [6]State Key Laboratory of Bioreactor Engineering, Biomedical Nanotechnology Center, Shanghai Collaborative Innovation Center for Biomanufacturing Technology, School of Biotechnology, East China University of Science and Technology, Shanghai 200237, P. R. China.
*Corresponding author. Email: wangcx@ibms.pumc.edu.cn (Chenxuan Wang); fangqj@nanoctr.cn (Q.F.)

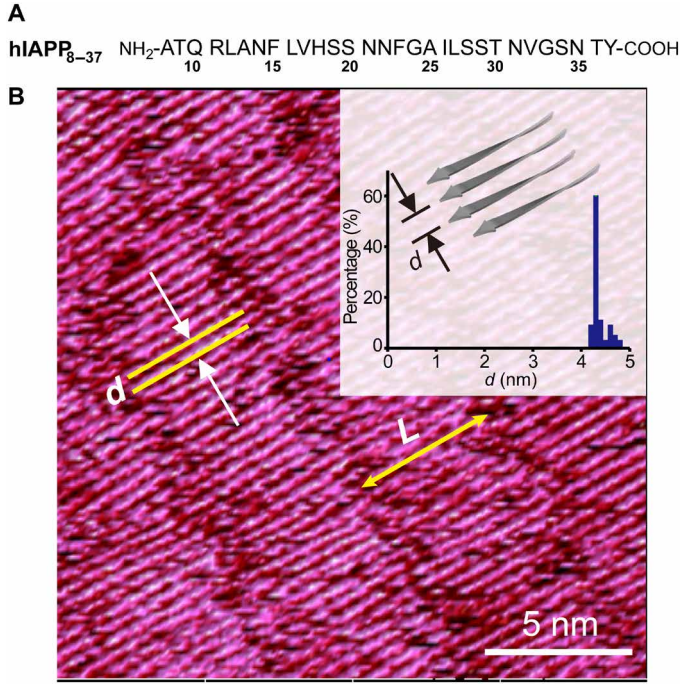

Fig. 1. Self-assembly of hIAPP$_{8–37}$ at HOPG surfaces. (**A**) Primary sequence of hIAPP$_{8–37}$. (**B**) A representative STM image of the hIAPP$_{8–37}$ self-assembly on the HOPG surface. Tunneling condition: I = 299.1 pA and V = 529.8 mV. The molecular axes of the hIAPP$_{8–37}$ peptide strands are indicated by the yellow double-headed arrow. The inset in (B) shows a statistical histogram of the d between the two adjacent peptide strands.

RESULTS

Self-assembly of hIAPP$_{8–37}$ at HOPG surfaces

Previous studies have shown that hIAPP exists in unstructured states under physiological conditions and misfolds into parallel β sheet structures that stack repetitively to form amyloidal fibrils in the pancreas of patients with type 2 diabetes (*15*–*17*). As evidenced in our experiments, the conversion of unstructured hIAPP$_{8–37}$ monomers into misfolded β sheet–rich amyloid aggregates was indicated by the presence of amyloid fibrils with a variable length of several micrometers in aqueous solution (fig. S1). To gain more structural information, we deposited a 0.4 mM hIAPP$_{8–37}$ aqueous solution on an HOPG surface and used STM to determine the self-assembly structure of the hIAPP$_{8–37}$. As shown in Fig. 1B, the lines with bright contrast correspond to the core region of the hIAPP$_{8–37}$ peptide strands. The distance between the two adjacent peptide strands (d) was measured to be 4.3 ± 0.2 Å (Fig. 1B and table S1), which is generally consistent with the interstrand spacing between two neighboring hydrogen bond–linked peptide strands of characteristic β sheet secondary structures (*18*). Therefore, we conclude that at the HOPG surface, hIAPP$_{8–37}$ molecules adopt a hydrogen-bonded β conformation and self-assemble into β sheets, where the successive side chains within one peptide strand alternately extend to the two opposite sides of a pleated lamina. Our observations are consistent with prior cryo–electron microscopy and electron paramagnetic resonance spectroscopy experiments that showed that hIAPP fibrils have an ordered parallel cross-β structure and are composed of multiple β strand motifs (*19*, *20*). We comment that the accurate measurement of the length of peptide strands (L) is not feasible because it is difficult to distinguish the peptide termini from the STM image.

Adsorption of ThT at the hIAPP$_{8–37}$ assembly surface

To understand the binding of ThT to hIAPP$_{8–37}$, we deposited a mixture solution of 0.4 mM hIAPP$_{8–37}$ and 1 mM ThT on an HOPG surface, and we investigated the coassembly structure of hIAPP$_{8–37}$ and ThT using the same STM conditions. As shown in Fig. 2A, the size of a single ThT is expected to be 1.3 nm × 0.4 nm (length × width), which is supported by the cocrystal structure of monomeric ThT with *Torpedo californica* acetylcholinesterase (Protein Data Bank ID: 2J3Q) (*21*). Past studies have shown that free ThT in solution presents a wide distribution of conformations from the perpendicular state (the torsion angle φ between the benzothiazole and the benzylamine moieties is 90°) to the planar state (φ = 0°; Fig. 2A) (*22*, *23*). As shown in the STM image of the hIAPP$_{8–37}$/ThT binary coassembly (Fig. 2B), the signals of the ThT molecules were ambiguous, which is possibly due to the thermal fluctuation of ThT atop the hIAPP$_{8–37}$ assembly. This observation is also supported by the quantification of the contrast of the brightness of ThT molecules. The cross-sectional profile analysis indicates that the difference in height (Δh) from the peak (ThT molecule) to the valley (substrate surface) was calculated to be 92 pm, which is indistinguishable.

Coassembly of a chaperone-like molecule and hIAPP$_{8–37}$ at HOPG surfaces

To decrease the thermal fluctuation of the hIAPP$_{8–37}$/ThT binary coassembly system, we introduced a chaperone-like molecule to coordinate with hIAPP$_{8–37}$ to increase the crystallinity of the protein assembly. Our previous studies have demonstrated that a chaperone-like molecule, 4,4′-bipyridine (4Bpy; Fig. 3A), forms hydrogen bonding with the carboxyl termini of peptides, resulting in a reduction in the thermal fluctuations of the peptide pattern on the surface (*24*, *25*). In our experiments, a mixture of 0.4 mM hIAPP$_{8–37}$ and 0.4 mM 4Bpy was deposited on an HOPG surface, and the hIAPP$_{8–37}$/4Bpy coassembly was visualized by using STM (Fig. 3B). In the hIAPP$_{8–37}$ sequence, there is no aspartic acid (Asp) or glutamic acid (Glu) that carries a carboxylic acid group that would potentially interact with 4Bpy via forming COOH···N hydrogen bonds. Thus, we expect that 4Bpy exclusively interacts with the hIAPP$_{8–37}$ strand via forming an N···H—O hydrogen bond between the nitrogen atom of 4Bpy and the C-terminal carboxyl moiety of the peptide (Fig. 3B). As evidenced in the representative STM image (Fig. 3), the linear arrays with the relatively higher level of brightness correspond to 4Bpy strings, which have a higher electron density of states. The width of the bright features was measured to be approximately 0.8 nm, consistent with the theoretical size of a 4Bpy molecule. Between the two adjacent strings of 4Bpy, the lamella features with lower contrast are assigned to the hIAPP$_{8–37}$ peptide strands. The separation between two neighboring peptide strands has been measured to be 5.2 ± 0.2 Å in the hIAPP$_{8–37}$/4Bpy coassembly. This interstrand separation is slightly larger than 4.3 ± 0.2 Å for the hIAPP$_{8–37}$ self-assembly but still within the distance range of hydrogen bond formation (*20*).

We reason that the location of 4Bpy labels the C termini of peptides and thereby provides a quantitative measure of the length of β-motifs in hIAPP$_{8–37}$ strands to deduce the polypeptide folding sites. As illustrated in Fig. 3B and table S3, the length ranges from 3.8 to 5.0 nm for the hIAPP$_{8–37}$ C-terminal β-motifs. A previous study has reported the separation between two neighboring residues within

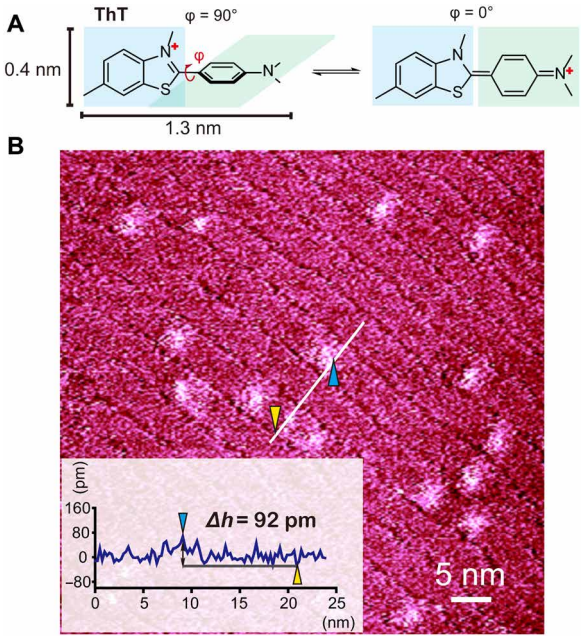

Fig. 2. Adsorption of ThT on hIAPP$_{8–37}$ monolayer self-assembly. (**A**) Perpendicular (left) and planar (right) resonance forms of ThT with the torsion angle φ between the benzothiazole and the benzylamine moieties. The blue and green planes represent the planes of the benzothiazole and the benzylamine moieties, respectively. The torsion angle φ is the dihedral angle between these two planes. (**B**) Representative STM image of hIAPP$_{8–37}$/ThT coassembly on the surface of HOPG. Tunneling condition: I = 299.1 pA and V = 589.0 mV. Cross-sectional profiles corresponding to the white line in (B). The blue and yellow triangles label the peak and the valley, respectively.

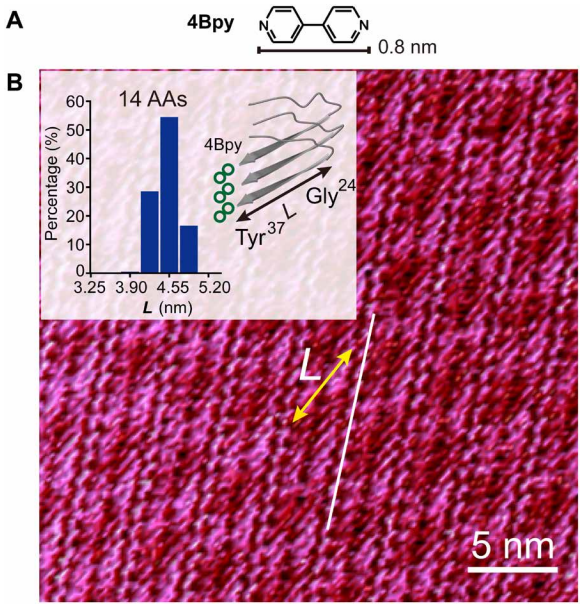

Fig. 3. Coassembly of hIAPP$_{8–37}$/4Bpy at HOPG surfaces. (**A**) Molecular structure of 4Bpy. (**B**) Representative STM image of the coassembly of hIAPP$_{8–37}$/4Bpy at HOPG surfaces. Tunneling condition: I = 299.1 pA and V = 539.2 mV. The yellow and white lines depict the molecular axis of the hIAPP$_{8–37}$ strand and the string composed of 4Bpy molecules, respectively. Inset in (B) shows the distribution of L of hIAPP$_{8–37}$ and the proposed structure of the coassembly of hIAPP$_{8–37}$/4Bpy. AAs, amino acids.

one main chain to be 0.325 nm in the parallel β sheet structures (*18*). Accordingly, we estimate the residue number of the amino acids for the core region of hIAPP$_{8–37}$ to be 12 to 15, and the most probable C-terminal β-motif length corresponds to 14 amino acid residues. On the basis of these calculation, the majority of the hIAPP$_{8–37}$ C-terminal β-motifs were determined to be Gly^{24}-Tyr^{37} (54.5% in the population), while a small population of C-terminal β-motif was observed to be Ile^{26}-Tyr^{37} (0.4%), Ala^{25}-Tyr^{37} (28.5%), and Phe^{23}-Tyr^{37} (16.6%). Moreover, the multiplicity of hIAPP$_{8–37}$ folding structures suggests that the hIAPP$_{8–37}$ molecules in the STM image are a polymorphic mixture composed of multiple discrete conformers. We also note that, in the hIAPP$_{8–37}$/4Bpy STM image (Fig. 3B), the N-terminal domain, Ala^{8}-Gly^{24}, of hIAPP$_{8–37}$ was indiscernible. We hypothesize that the N-terminal domain of hIAPP$_{8–37}$ is positioned >1 nm to the HOPG surface, which exceeds the separation distance that allows electrons to tunnel through the gap between the STM tip and a substrate (*26*).

Ternary coassembly of ThT and hIAPP$_{8–37}$ with 4Bpy

To verify the impacts of protein substrate crystallinity on modulating ThT adsorption, we prepared the ternary coassembly of hIAPP$_{8–37}$/4Bpy/ThT by depositing a drop of the mixed aqueous solution containing 0.4 mM hIAPP$_{8–37}$, 0.4 mM 4Bpy, and 1 mM ThT on an HOPG surface for STM imaging. Intriguingly, dozens of the fusiform and quadrilaterals with high brightness contrast were formed between the 4Bpy strings in this ternary coassembly system, as shown in Fig. 4 (A to D). Theoretically, the conjugated π electrons of the benzylamine and benzathiole moieties of ThT have a relatively high local electron density of states in STM imaging, and thereby, the fusiform and quadrilaterals are attributed to be the adsorbed ThT molecules. As shown in the cross-sectional profile in Fig. 4A, the center section of the curve presents a plateau with a clear boundary, corresponding to ThT molecules. The Δh of the plateau is measured to be 186 pm, which is higher than that of an hIAPP$_{8–37}$/ThT coassembly (92 pm; Fig. 4E). These results support our hypothesis that 4Bpy enhances the crystallinity of hIAPP$_{8–37}$ lamella and, thus, reduces the thermal fluctuations of ThT, resulting in improvements in the resolution of ThT molecules under STM.

Selective oligomerization of ThT atop an hIAPP$_{8–37}$/4Bpy coassembly

In the STM images of the hIAPP$_{8–37}$/4Bpy/ThT ternary system, the sizes of the fusiform and quadrilaterals formed by ThT molecules were measured to be a set of discrete amounts in the range of 1.5 nm × 0.9 nm to 2.3 nm × 1.5 nm, which are substantially larger than the theoretical molecular size of a single ThT molecule. This observation reveals that ThT molecules are bound as oligomers on the β sheet platelet formed by hIAPP$_{8–37}$. To provide more insights into the oligomerization state of ThT, we used an STM tip to remove part of a fusiform from its original location without disruption of the rest of the coassembly structure, as shown in Fig. 4 (F and G). The states of ThT oligomers were subsequently investigated on the basis of their geometrical characteristics. We observed most of the ThT oligomers aligning along the axes of hIAPP$_{8–37}$ β strands. Thus, we defined the side length of ThT oligomers parallel and perpendicular to the axes of the peptide strand to be L and W, respectively. Given the expected size of a single ThT molecule (approximately 1.3 nm × 0.4 nm),

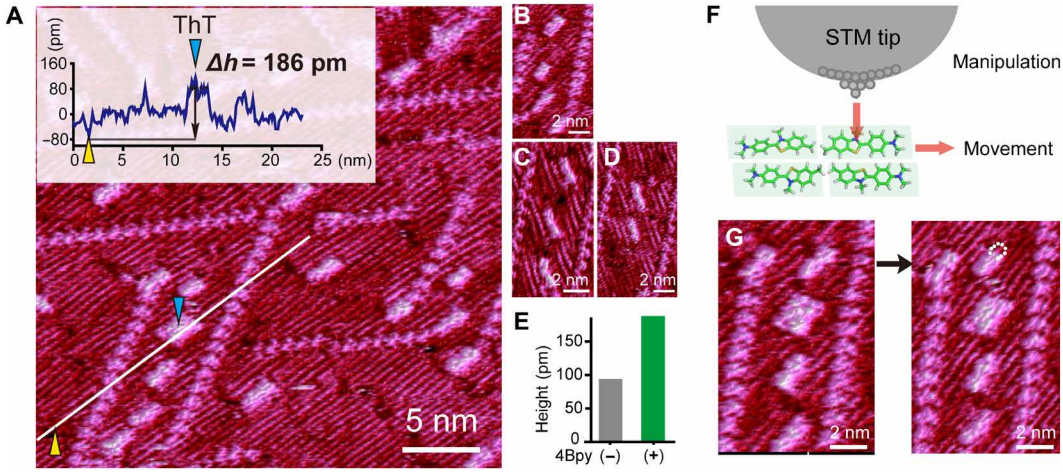

Fig. 4. Selective oligomerization of ThT atop hIAPP$_{8–37}$ with 4Bpy. (**A** to **D**) Representative STM image of ThT adsorption at hIAPP$_{8–37}$/4Bpy surfaces. Tunneling conditions: I = 299.1 pA and V = 519.4 mV. Inset in (A) represents the cross-sectional profile corresponding to the white line. The blue and yellow triangles label the peak and the valley in (A). (**E**) STM contrast of ThT in the absence (gray) or presence (green) of 4Bpy. (**F** and **G**) Scheme and STM images of ThT oligomers before (left) (G) and after (right) (G) removal of ThT molecules. The dashed circle highlights the part removed by the STM tip.

four types of ThT oligomers were identified and summarized in Fig. 5A.

Figure 5A shows the representative morphologies and the proposed molecular models for each oligomerization state. In the first type of ThT oligomers (approximately 1.3 nm × 0.9 nm), the W of an oligomer, 0.9 nm, is approximately equivalent to twice the short molecular axis of ThT. Thus, we attributed this type of ThT oligomer to be a "1 × 2" mode, which indicates that two ThT molecules are organized with a side-by-side configuration atop the surface of hIAPP$_{8–37}$ strands. Moreover, the long molecular axes of ThT were observed to be parallel with the peptide strands. Similarly, the second type of ThT oligomers (2.3 nm × 0.5 nm) was assigned to the "2 × 1" mode where two ThT molecules are packed in a head/tail configuration. Following the same analysis method, the assembly modes "2 × 2" and "2 × 3" were determined for the other two types of ThT oligomers observed in STM images. In summary, the aggregation numbers for each association state were determined to be dimer (1 × 2 and 2 × 1), tetramer (2 × 2), and hexamer (2 × 3). Two conclusions can be drawn from our experiments. First, the oligomerization states of ThT are exclusively even numbers (dimer, tetramer, and hexamer) instead of odd numbers (monomer, trimer, etc.). Second, there exists a selection role for the ThT oligomerization state. This conclusion can be drawn due to a lack of observation of some types of oligomerization states. Specifically, the "1 × 4" or "4 × 1" oligomers have not been observed in our STM observations.

Contribution of cohesive interactions in ThT oligomerization

In this section, we calculate the free energy of the 1 × 2, 2 × 1, and 2 × 2 states based on a statistical distribution of ThT oligomers. As shown in Fig. 5 (B and C) and table S4, the number distribution of ThT was obtained on the basis of the population of ThT oligomers. The probability theory relates the probability (P_i) of the system being in state i to the energy of that state (E_i) and the temperature of the system (T) as (*27*)

$$P_i = \frac{e^{-E_i/k_BT}}{\sum_{j=1}^{M} e^{-E_j/k_BT}} \quad (1)$$

where k_B is the Boltzmann constant and M is the number of all states accessible to the system. The relative energy difference between two states depends on the ratio of their probabilities

$$E_i - E_j = -k_BTln\left(\frac{P_i}{P_j}\right) \quad (2)$$

As shown in Fig. 5D, the relative energy difference between the 1 × 2, 2 × 1, and 2 × 2 states was calculated by using Eq. 2. To relate the relative energy difference to the cohesion work, we have

$$2E_{2\times1} - 2E_{1\times2} = W_{\text{co-side}} - W_{\text{co-head}} = -2.2\,k_BT \quad (3)$$

$$4E_{2\times2} - 4E_{2\times1} = 2W_{\text{co-head}} - (2W_{\text{co-head}} + 2W_{\text{co-side}}) = -8.4\,k_BT \quad (4)$$

in which $E_{1\times2}$, $E_{2\times1}$, and $E_{2\times2}$ are the free energy per ThT molecule in the 1 × 2, 2 × 1, and 2 × 2 states, respectively. $W_{\text{co-head}}$ and $W_{\text{co-side}}$ are the cohesion work needed to separate two ThT molecules that are in head/tail contact and side-by-side contact, respectively (Fig. 5E). In our calculation, we use the singly dispersed ThT adsorbed at the hIAPP$_{8–37}$ surface as the reference state, so the cohesion work is positive.

By combining Eqs. 3 and 4, we calculated $W_{\text{co-head}}$ and $W_{\text{co-side}}$ to be 6.4 and 4.2 k_BT, respectively. This result provides insights into the role of the cohesive interaction between ThT molecules in their selective oligomerization. For instance, we can estimate the free energy difference among three possible tetramer structures

$$4E_{1\times4} - 4E_{2\times2} = (2W_{\text{co-head}} + 2W_{\text{co-side}}) - 3W_{\text{co-side}} = 8.6\,k_BT \quad (5)$$

$$4E_{4\times1} - 4E_{2\times2} = (2W_{\text{co-head}} + 2W_{\text{co-side}}) - 3W_{\text{co-side}} = 2.0\,k_BT \quad (6)$$

These calculation results support our experimental observation that the formation of 2 × 2 oligomers is more favorable in energy than the formation of 1 × 4 and 4 × 1 oligomers (Fig. 5G).

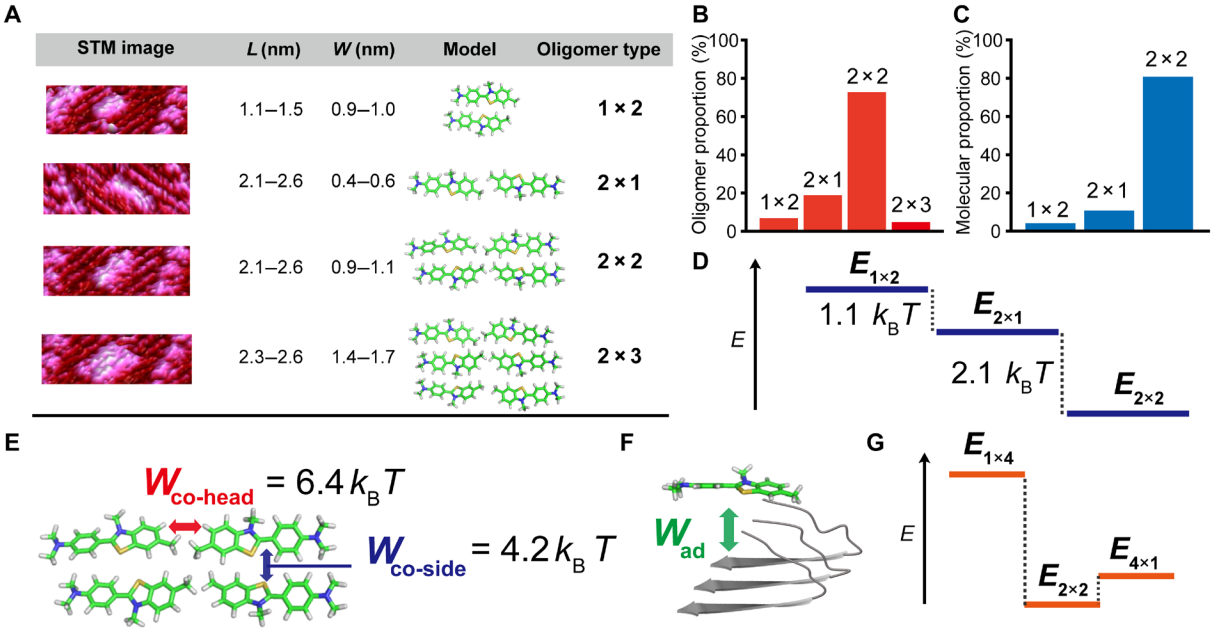

Fig. 5. Oligomerization states of ThT on hIAPP$_{8–37}$. (**A**) Measured and simulated oligomerization states of ThT on hIAPP$_{8–37}$/4Bpy coassembly surfaces. (**B** and **C**) Number distribution of different types of ThT oligomers determined by (B) the number of oligomers and (C) the number of constituent ThT units. (**D**) Relative energy difference between 1 × 2, 2 × 1, and 2 × 2 oligomerization states. (**E** and **F**) Schematic illustration of (E) cohesive interactions within a 2 × 2 ThT tetramer and (F) adhesive interactions between a ThT monomer and protein substrate. Color codes for (E) and (F): green for carbon, yellow for sulfur, blue for nitrogen, white for hydrogen, and gray for hIAPP$_{8–37}$. (**G**) A schematic illustration of relative energy difference between the 2 × 2, 1 × 4, and 4 × 1 states.

Before describing the results regarding adhesive interactions, we make four statements. First, our STM imaging was performed with an equilibration time over 24 hours, and thus, the resulting interfacial adsorption and self-assembly of ThT molecules are regarded to be at equilibrium, which allows us to relate the energy of each oligomerization state with the occurring probability. Second, considering that ThT oligomers mostly adsorbed in the middle portion of the peptide strands, the possibility that the adhesion work (W_{ad}) to separate a ThT from the peptide assembly (Fig. 5F) may be different due to the variation of ThT-binding sites on the hIAPP$_{8–37}$ assembly surface was not taken into account. Third, it is difficult to distinguish the molecular conformation of a single ThT within an oligomer based on the current resolution. Last, the ThT concentration in STM observations, 1 mM, is relatively low and might influence the number of 2 × 3 oligomers to deviate from the equilibrium state. Thus, the small number of ThT molecules at the 2 × 3 oligomerization states was not considered in the number distribution of ThT. In the future, we will increase the concentration of ThT to investigate the number distributions of ThT with higher association numbers.

Role of adhesive interactions on ThT oligomerization

As demonstrated in our STM experiments, the segment of the C-terminal domain Gly^{24}-Tyr^{37} of hIAPP with the sequence GAILSSTNVGSNTY is involved in the interactions between the adsorbed ThT and the hIAPP$_{8–37}$ assembly. Specifically, most ThT molecules bind in the middle region of the Gly^{24}-Tyr^{37} motifs, rather than the proximity of the peptide C termini, i.e., Tyr^{37}. Therefore, the adsorption of ThT is driven by the attractive interaction generated by the side chains of the Gly^{24}-Thr^{36} segment, which can be categorized into two groups according to their pertinent properties, such as a polar and uncharged group (Ser, Thr, and Asn) and a nonpolar group (Ala, Ile, Leu, and Val). The sulfur atom of ThT is a weak hydrogen bond acceptor in comparison with the conventional N—H···O, O—H···O, and O—H···N hydrogen bonds (*28*), whereas the delocalization of the sulfur electron pair in the benzothiazole ring further weakens the hydrogen-bonding capability of the sulfur atom of ThT. Thus, the intermolecular interactions between ThT and the Gly^{24}-Thr^{36} segment are mainly attributed to being van der Waals interactions and hydrophobic interactions. We predict that there exists a change of the intermolecular interactions controlled by the surface of the two-dimensional polypeptide substrate, e.g., adding electrostatic attractions to change the adsorbed ThT orientation, which results in a different adhesive interaction between ThT and the peptide substrate and, thus, changes the oligomerization state of the bounded ThT.

DISCUSSION AND CONCLUSION

In this work, our STM experimental approaches provide detailed information at a molecular level and leverage the knowledge gained to control the oligomerization of drug molecules at their protein receptors. On the planar surface of a two-dimensional protein assembly system, we revealed that the binding structures of ThT involve multiple association states, including dimers in two packing configurations (1 × 2 and 2 × 1), tetramers (2 × 2), and hexamers (2 × 3). Tetramers are a quantitatively dominant oligomer, where the long axes of ThT molecules are parallel to the main chains of hIAPP$_{8–37}$. Multiple binding states of ThT were ranked by their respective occurring frequency, which is reflected by the difference in energy between states. The different association states of ThT reflect changes in the intermolecular interactions between adjacent ThT molecules (cohesive interactions) and interactions between ThT and the protein substrate (adhesive interactions). Specifically, the

work of cohesive interactions required to separate two ThT molecules, in head/tail contact and side-by-side contact, was calculated to be 6.4 and 4.2 k_BT, respectively. In addition, we demonstrate that the work of adhesive interactions between ThT and the receptor depends on the microenvironment of the binding site. In contrast to the ambiguous STM signal of ThT adsorbed at the $hIAPP_{8–37}$ surface (Fig. 2B), the resolution of the STM images of ThT at the 4Bpy/$hIAPP_{8–37}$ assembly surface is enhanced, allowing a better understanding of the locations of the ThT oligomers (Fig. 4A). In addition, ThT oligomers are prone to adsorb atop the 4Bpy-rich region rather than the 4Bpy-lean region (as shown in Fig. 4A). These observations lead us to conclude that the work of adhesive interactions between ThT and the receptor depends on the microenvironment of the binding site (i.e., pure $hIAPP_{8–37}$ surface versus 4Bpy/$hIAPP_{8–37}$ coassembly).

We believe that our work provides a new principle for the design of the oligomerization state of bounded drugs for future studies. We expect to use a small molecule–assembled nanocluster to occupy a large binding pocket instead of creating a large molecule with high molecular weight. The ability to select the oligomerization state will provide a number of advantages that would benefit drug targeting, such as the improvement of local drug concentration without conjugating drugs via covalent interactions that can potentially change the drug function, the cooperation between different subunits of an oligomer enabling a cooperative activation in the molecular recognition process, and the increased stability of drugs against proteolytic degradation due to the reduced surface area of drug exposed to the solvent and enzymes.

This report also provides single molecular evidence that the use of a chaperone-like molecule is a feasible strategy for STM visualization of a drug ligand bound to its receptor. Many challenges and debates remain on the molecular mechanism by which drug molecules bind with amyloids due to the limited resolution of conventional structural characterization methods (*8*, *29*–*33*). STM provides direct molecular imaging to determine the structural characteristics and the critical drug-binding sites in the intrinsic heterogeneous protein systems where conventional techniques (e.g., x-ray crystallography, nuclear magnetic resonance spectroscopy, and cryo–electron microscopy) that average or extract only periodic information of the structures are restricted. The chaperone-assisted strategy can be propagated into the field of study on the bound state of a drug molecule that involves a switch between multiple metastable configurations and the interactions of drug candidates with either intrinsically disordered proteins or proteins that contain multiple conformers. Currently, the mechanism by which a chaperone-like molecule decreases the thermal fluctuation of a drug ligand has yet to be understood. The first possible mechanism is proposed as "direct" intermolecular interactions occurring between chaperones and drugs. Detailed studies of a variety of guest molecules adsorbed on the supramolecular host structure illustrate that the weak intermolecular interactions between guest and host species, such as van der Waals interactions and hydrogen bonds, are known to confine the diffusion of the guest molecule (*34*–*36*). Given the fact that no direct, noncovalent interaction between ThT and 4Bpy was observed in the ternary structures of ThT/$hIAPP_{8–37}$/4Bpy, this direct mechanism appears unlikely to account for our experimental observations. Alternatively, the second possible mechanism involves an "indirect" interaction—the periodic 4Bpy arrays play a spatial confinement effect that increases the crystallinity of protein assemblies on a molecular scale and thus reduce the diffusion of ThT on the $hIAPP_{8–37}$ surface. We comment here that the structure of $hIAPP_{8–37}$ folding and assembly determined by our STM is in quantitative agreement with previous in vivo study (*37*–*39*) and the structure determined using other conventional characterization techniques such as x-ray crystallography and nuclear magnetic resonance spectroscopy (*17*, *40*).

As a summary, our fundamental studies draw attention to a previously unidentified molecular recognition mechanism where a drug molecule adopts different oligomerization states to interact with specific proteins. Distinct from the conventional lock-and-key concept of probe binding as a monomer, our observations lead to a novel proof of concept that ThT oligomers act as an indivisible unit to recognize their target. The adhesive interactions and cohesive interactions endow ThT with a unique oligomerization state selectivity. We will explore the impacts of the chemical context of side chains on ThT oligomerization in our future studies by using the two-dimensional peptide assembly system to exclusively present charged side chains or aromatic side chains. These fresh single-molecule insights provide pathways for understanding the precise manipulation of the association states of a drug molecule in a complex biological system and will inspire the design of drug compounds based on the concept of oligomer state-dependent recognition.

MATERIALS AND METHODS

Materials

Lyophilized powders of synthetic $hIAPP_{8–37}$ were purchased from the Bankpeptide Biological Technology Co. Ltd. The purity of peptide powders (above 98%) was verified by high-performance liquid chromatography and mass spectroscopy. ThT, 4Bpy, and hexafluoroisopropanol (HFIP) were purchased from Sigma-Aldrich Co. Ltd. These chemicals were of analytical grade and, hence, used without any further purification.

Preparation of STM samples

Lyophilized powders of $hIAPP_{8–37}$ were dispersed in HFIP to obtain unfolded $hIAPP_{8–37}$ monomers. After the HFIP was evaporated, the peptide was dissolved in Milli-Q water to achieve a concentration of 0.4 mM and was left to incubate in the water for 24 hours. Similarly, for the samples of the $hIAPP_{8–37}$/ThT, $hIAPP_{8–37}$/4Bpy, and $hIAPP_{8–37}$/ThT/4Bpy coassemblies, the peptides were added with the corresponding small molecules to form the corresponding solutions. The final concentrations of $hIAPP_{8–37}$, ThT, and 4Bpy were 0.4, 0.4, and 1 mM, respectively. The mixed solutions were incubated in Milli-Q water for 24 hours. A 10-μl sample of each solution was then deposited on separate surfaces of freshly cleaved HOPG. After incubating for 20 min, the excess solution was removed from the HOPG surface by high-purity nitrogen gas. Interfacial water films were then formed on the surface of the HOPG to create a liquid-solid interface.

STM measurements

STM experiments were performed in the constant-current mode under ambient conditions (Nanoscope IIIa SPM system, Bruker, USA). The STM tips were mechanically formed using Pt/Ir wire (80/20). The tunneling conditions are described in the corresponding figure captions. In practice, however, the results from the STM measurements also depend on the STM tip geometry. It is nearly impossible to control the geometry of each STM tip at the atomic scale. To distinguish if there are any artifacts in the STM images generated by

a specific STM tip, experiments were repeated independently using different tips. This was done to ensure the reproducibility of measurements. The specific features of peptide strands in the STM images had a certain amount of variability, which resulted from variability in the STM tips in combination with the molecular conformational fluctuations. The results on the statistical distribution of the length, however, were nearly unaffected by different sample preparation conditions.

Statistical methods

The lengths of the peptide strands in the STM images were measured by using the Gwyddion software (version 2.31, Czech Metrology Institute, Czech Republic). A length increment of 0.325 nm is assumed in the statistical histogram of the length distribution of peptide assemblies. The measured lengths in the histograms represent 200 to 300 measured values from the STM images. The number frequencies in the statistical results are all based on the number of events. Assignments of the most probable sites are determined from the peak distribution of peptide length histograms.

Molecular simulation

To illustrate the molecular arrangement of ThT oligomers, theoretical calculations were performed in a vacuum using a dispersion-corrected density functional theory (DFT-D) scheme provided by the DMol3 code (*41*). The Perdew-Burke-Ernzerhof parameterization of the local exchange-correlation energy was applied to describe the exchange and correlation. All-electron spin-unrestricted Kohn-Sham wave functions were expanded in a local atomic orbital basis. For the large system, the numerical basis set was applied. All calculations were all-electron ones and were performed with the medium mesh. The self-consistent field procedure was performed with a convergence criterion of 10^{-5} arbitrary units on the energy and electron density. The initial models were built on the basis of experimental lattice parameters. Then, DFT calculations were performed to further optimize these initial models in the perspectives of molecular configuration and lattice parameters. More information is provided in section S1.

SUPPLEMENTARY MATERIALS

Supplementary material for this article is available at http://advances.sciencemag.org/cgi/content/full/6/32/eabc1449/DC1

View/request a protocol for this paper from *Bio-protocol*.

REFERENCES AND NOTES

1. W. D. Kohn, C. M. Kay, R. S. Hodges, Orientation, positional, additivity, and oligomerization-state effects of interhelical ion pairs in alpha-helical coiled-coils. *J. Mol. Biol.* **283**, 993–1012 (1998).
2. D. S. Goodsell, A. J. Olson, Structural symmetry and protein function. *Annu. Rev. Biophys. Biomol. Struct.* **29**, 105–153 (2000).
3. R. Nussinov, H. Jang, C. J. Tsai, Oligomerization and nanocluster organization render specificity. *Biol. Rev. Camb. Philos. Soc.* **90**, 587–598 (2015).
4. B. Ciani, S. Bjelic, S. Honnappa, H. Jawhari, R. Jaussi, A. Payapilly, T. Jowitt, M. O. Steinmetz, R. A. Kammerer, Molecular basis of coiled-coil oligomerization-state specificity. *Proc. Natl. Acad. Sci. U.S.A.* **107**, 19850–19855 (2010).
5. G. Meng, R. Fronzes, V. Chandran, H. Remaut, G. Waksman, Protein oligomerization in the bacterial outer membrane (review). *Mol. Membr. Biol.* **26**, 136–145 (2009).
6. G. Uguzzoni, S. John Lovis, F. Oteri, A. Schug, H. Szurmant, M. Weigt, Large-scale identification of coevolution signals across homo-oligomeric protein interfaces by direct coupling analysis. *Proc. Natl. Acad. Sci. U.S.A.* **114**, E2662–E2671 (2017).
7. S. R. Needham, S. K. Roberts, A. Arkhipov, V. P. Mysore, C. J. Tynan, L. C. Zanetti-Domingues, E. T. Kim, V. Losasso, D. Korovesis, M. Hirsch, D. J. Rolfe, D. T. Clarke, M. D. Winn, A. Lajevardipour, A. H. Clayton, L. J. Pike, M. Perani, P. J. Parker, Y. Shan, D. E. Shaw, M. L. Martin-Fernandez, EGFR oligomerization organizes kinase-active dimers into competent signalling platforms. *Nat. Commun.* **7**, 13307–13320 (2016).
8. C. Wu, M. T. Bowers, J. E. Shea, On the origin of the stronger binding of PIB over thioflavin T to protofibrils of the Alzheimer amyloid-beta peptide: A molecular dynamics study. *Biophys. J.* **100**, 1316–1324 (2011).
9. M. Biancalana, K. Makabe, A. Koide, S. Koide, Molecular mechanism of thioflavin-T binding to the surface of beta-rich peptide self-assemblies. *J. Mol. Biol.* **385**, 1052–1063 (2009).
10. P. C. Hiemenz, R. Rajagopalan, *Principles of Colloid and Surface Chemistry* (Marcel Dekker Inc., New York, 3rd., 1997).
11. R. K. Millen, S. C. Buhimschi, G. Zhao, M. K. Rood, S. Tabbah, A. I. Buhimschi, Serum and urine thioflavin-T-enhanced fluorescence in severe preeclampsia. *Hypertension* **71**, 1185–1192 (2018).
12. M. Groenning, M. Norrman, J. M. Flink, M. van de Weert, J. T. Bukrinsky, G. Schluckebier, S. Frokjaer, Binding mode of thioflavin T in insulin amyloid fibrils. *J. Struct. Biol.* **159**, 483–497 (2007).
13. M. Biancalana, S. Koide, Molecular mechanism of thioflavin-T binding to amyloid fibrils. *Biochim. Biophys. Acta* **1804**, 1405–1412 (2010).
14. M. Groenning, Binding mode of thioflavin T and other molecular probes in the context of amyloid fibrils-current status. *J. Chem. Biol.* **3**, 1–18 (2010).
15. T. J. Rink, K. Beaumont, J. Koda, A. Young, Structure and biology of amylin. *Trends Pharmacol. Sci.* **14**, 113–118 (1993).
16. A. V. Kajava, U. Aebi, A. C. Steven, The parallel superpleated beta-structure as a model for amyloid fibrils of human amylin. *J. Mol. Biol.* **348**, 247–252 (2005).
17. S. Luca, W.-M. Yau, R. Leapman, R. Tycko, Peptide conformation and supramolecular organization in amylin fibrils: Constraints from solid-state NMR. *Biochemistry* **46**, 13505–13522 (2007).
18. R. H. Garrett., C. M. Grisham., *Biochemistry* (Saunders College Publishing: London, U.K., 2ed, 1999).
19. S. A. Jayasinghe, R. Langen, Identifying structural features of fibrillar islet amyloid polypeptide using site-directed spin labeling. *J. Biol. Chem.* **279**, 48420–48425 (2004).
20. O. S. Makin, L. C. Serpell, Structural characterisation of islet amyloid polypeptide fibrils. *J. Mol. Biol.* **335**, 1279–1288 (2004).
21. M. Harel, L. K. Sonoda, I. Silman, J. L. Sussman, T. L. Rosenberry, Crystal structure of thioflavin T bound to the peripheral site of *Torpedo californica* acetylcholinesterase reveals how thioflavin T acts as a sensitive fluorescent reporter of ligand binding to the acylation site. *J. Am. Chem. Soc.* **130**, 7856–7861 (2008).
22. S. Freire, M. H. de Araujo, W. Al-Soufi, M. Novo, Photophysical study of thioflavin T as fluorescence marker of amyloid fibrils. *Dyes Pigments* **110**, 97–105 (2014).
23. L. S. Wolfe, M. F. Calabrese, A. Nath, D. V. Blaho, A. D. Miranker, Y. Xiong, Protein-induced photophysical changes to the amyloid indicator dye thioflavin T. *Proc. Natl. Acad. Sci. U.S.A.* **107**, 16863–16868 (2010).
24. L. Yu, Y. Zheng, J. Xu, F. Qu, Y. Lin, Y. Zou, Y. Yang, S. L. Gras, C. Wang, Site-specific determination of TTR-related functional peptides by using scanning tunneling microscopy. *Nano Res.* **11**, 577–585 (2018).
25. X. B. Mao, C. X. Wang, X. K. Wu, X. J. Ma, L. Liu, L. Zhang, L. Niu, Y. Y. Guo, D. H. Li, Y. L. Yang, C. Wang, Beta structure motifs of islet amyloid polypeptides identified through surface-mediated assemblies. *Proc. Natl. Acad. Sci. U.S.A.* **108**, 19605–19610 (2011).
26. C. Wang, C. L. Bai, *Single Molecule Chemistry and Physics - An Introduction* (Springer, Germany, 2006).
27. A. McQuarrie, *Statistical mechanics* (University Science Books, California, 2000).
28. P. Zhou, F. Tian, F. Lv, Z. Shang, Geometric characteristics of hydrogen bonds involving sulfur atoms in proteins. *Proteins* **76**, 151–163 (2009).
29. R. Khurana, C. Coleman, C. Ionescu-Zanetti, S. A. Carter, V. Krishna, R. K. Grover, R. Roy, S. Singh, Mechanism of thioflavin T binding to amyloid fibrils. *J. Struct. Biol.* **151**, 229–238 (2005).
30. A. Sulatskaya, N. Rodina, M. Sulatsky, O. Povarova, I. Antifeeva, I. Kuznetsova, K. Turoverov, Investigation of α-synuclein amyloid fibrils using the fluorescent probe thioflavin T. *Int. J. Mol. Sci.* **19**, 2486–2502 (2018).
31. C. X. Wang, X. B. Mao, A. H. Yang, L. Niu, S. N. Wang, D. H. Li, Y. Y. Guo, Y. B. Wang, Y. L. Yang, C. Wang, Determination of relative binding affinities of labeling molecules with amino acids by using scanning tunneling microscopy. *Chem. Commun.* **47**, 10638–10640 (2011).
32. Z. Qin, Y. Sun, B. Jia, D. Wang, Y. Ma, G. Ma, Kinetic mechanism of thioflavin T binding onto the amyloid fibril of hen egg white lysozyme. *Langmuir* **33**, 5398–5405 (2017).
33. N. Iwakawa, D. Morimoto, E. Walinda, Y. Kawata, M. Shirakawa, K. Sugase, Real-time observation of the interaction between thioflavin T and an amyloid protein by using high-sensitivity Rheo-NMR. *Int. J. Mol. Sci.* **18**, 2271–2278 (2017).
34. S. B. Lei, S. X. Yin, C. Wang, L. J. Wan, C. L. Bai, Selective adsorption of copper phthalocyanine atop functionalized organic monolayers. *J. Phys. Chem. B* **108**, 224–227 (2004).

35. D. X. Wu, K. Deng, Q. D. Zeng, C. Wang, Selective effect of guest molecule length and hydrogen bonding on the supramolecular host structure. *J. Phys. Chem. B* **109**, 22296–22300 (2005).
36. J.-H. Tang, Y. Li, Q. Wu, Z. Wang, S. Hou, K. Tang, Y. Sun, H. Wang, H. Wang, C. Lu, X. Wang, X. Li, D. Wang, J. Yao, C. J. Lambert, N. Tao, Y.-W. Zhong, P. J. Stang, Single-molecule level control of host-guest interactions in metallocycle-C60 complexes. *Nat. Commun.* **10**, 4599–4607 (2019).
37. P. Westermark, Fine structure of islets of langerhans in insular amyloidosis. *Virchows Arch. A Pathol. Pathol. Anat.* **359**, 1–18 (1973).
38. G. J. S. Cooper, A. C. Willis, A. Clark, R. C. Turner, R. B. Sim, K. B. M. Reid, Purification and characterization of a peptide from amyloid-rich pancreases of type-2 diabetic-patients. *Proc. Natl. Acad. Sci. U.S.A.* **84**, 8628–8632 (1987).
39. D. Raleigh, X. Zhang, B. Hastoy, A. Clark, The beta-cell assassin: IAPP cytotoxicity. *J. Mol. Endocrinol.* **59**, R121–R140 (2017).
40. J. J. W. Wiltzius, S. A. Sievers, M. R. Sawaya, D. Cascio, D. Popov, C. Riekel, D. Eisenberg, Atomic structure of the cross-beta spine of islet amyloid polypeptide (amylin). *Protein Sci.* **17**, 1467–1474 (2008).
41. J. P. Perdew, K. Burke, M. Ernzerhof, Generalized gradient approximation made simple. *Phys. Rev. Lett.* **77**, 3865–3868 (1996).

Acknowledgments
Funding: C.W. thanks the CAMS Innovation Fund for Medical Sciences (2018-I2M-3-006), the National Natural Science Foundation of China (31901007), the Fundamental Research Funds for the Central Universities (2018PT31028), the Open Project Fund provided by the Key Laboratory for Biomedical Effects of Nanomaterials and Nanosafety, the CAS (NSKF201812), the State Key Laboratory Special Fund 2060204, and the Natural Science Foundation of Shanghai (19ZR1412400). We also thank the National Center for Nanoscience and Technology, China, for STM facilities, and X. Mao (Johns Hopkins University) for discussion. **Author contributions:** L.Y., W.Z., Y.Y., Chen Wang, and Chenxuan Wang designed the project, performed the STM experiments, and wrote the manuscript. W.L., B.T., and Q.F. performed molecular simulation and discussed the data. R.L.D., Y.X., Y.W., H.X., X.W., Q.F., Y.Y., and C.W. discussed the data and modified the manuscript. **Competing interests:** Chenxuan Wang, L.Y., Chen Wang, and Y.Y. are inventors on a pending Chinese patent related to this work filed by the Chinese Academy of Medical Sciences and the Peking Union Medical College (application no. 202010070997.3). The authors declare that they have no other competing interests. **Data and materials availability:** All data needed to evaluate the conclusions in the paper are present in the paper and/or the Supplementary Materials. Additional data related to this paper may be requested from the authors.

Submitted 8 April 2020
Accepted 22 June 2020
Published 5 August 2020
10.1126/sciadv.abc1449

Citation: L. Yu, W. Zhang, W. Luo, R. L. Dupont, Y. Xu, Y. Wang, B. Tu, H. Xu, X. Wang, Q. Fang, Y. Yang, Chen Wang, Chenxuan Wang, Molecular recognition of human islet amyloid polypeptide assembly by selective oligomerization of thioflavin T. *Sci. Adv.* **6**, eabc1449 (2020).